Journal of Applied Polymer Science

SANS Studies on Catalyst Ink of Fuel Cell

Mitsuhiro Shibayama,[1] Takuro Matsunaga,[1] Takumi Kusano,[1] Kazuki Amemiya,[2] Noriyuki Kobayashi,[2] Toshihiko Yoshida[2]

[1]Neutron Science Laboratory, Institute for Solid State Physics, U. Tokyo, Kashiwa, Chiba 277-8581, Japan
[2]FC Development Center, Toyota Motor Corporation, Higashifuji Technical Center, Susono, Shizuoka 411-1193, Japan
Correspondence to: M. Shibayama (E-mail: sibayama@issp.u-tokyo.ac.jp)

ABSTRACT: The structure of solid polymer electrode and catalyst ink of fuel cell has been investigated by focusing- (FSANS) and contrast-variation small-angle neutron scattering (CV-SANS). The solid polymer electrode, consisting of carbon (C), platinum, and ionomer (polymer, P), exhibited a power-law function with two asymptotes, i.e., from $I(q) \sim q^{-1}$ to $I(q) \sim q^{-4}$ with a crossover around $q \approx 0.005$ Å^{-1}. The scattering functions of the catalyst ink, i.e., the polymer electrodes dispersed in water, were successfully decomposed to the corresponding partial structure factors, $S_{CC}(q)$, $S_{PP}(q)$, $S_{CP}(q)$, exclusively representing C-C, P-P, and C-P correlations. $S_{CC}(q)$ was a monotonic decreasing function of q, dominating in the scattering from carbon clusters. On the other hand, $S_{PP}(q)$ exhibited a scattering maximum characteristic of polyelectrolyte solutions. This suggests that ionic clusters in polyelectrolyte solutions are formed in catalyst ink. The cross term, $S_{CP}(q)$, indicated that the carbon scattering is dominant and significant amount of ionomer is adsorbed on the carbon agglomerates. It is concluded that the catalyst ink consists of carbon agglomerates surrounded by ionomers and the presence of ionic-cluster path plays a key role in the performance of the solid polymer electrodes in polymer electrolyte fuel cells. © 2013 Wiley Periodicals, Inc. J. Appl. Polym. Sci. **2014**, *131*, 39842.

KEYWORDS: fuel cell; catalyst ink; small-angle neutron scattering; contrast variation; polyelectrolyte

Received 4 December 2012; accepted 11 August 2013
DOI: 10.1002/app.39842

INTRODUCTION

Development of fuel cells has been a hot topic in materials science.[1] The performance of fuel cells depends greatly on its electrodes and separator. Recently, polymer electrode fuel cells (PEFCs) have been gathering much attention due mainly to their high power density, compactness, high performance by cost, quick and stable operation at low temperatures (room temperature to 100°C), nonelectrolyte leakage, and so on. Hence, PEFCs are now one of the most potential candidates for applications such as transportation, portable power generators, and generators for houses and buildings.

Perfluorosulfonate ionomer (PFSI) membranes, such as Nafion® membranes, have been most commonly used for the proton exchange membrane of fuel cells. Intensive researches have been carried out on the structure and properties of Nafion and/or other perfluorocarbon membranes by X-ray or neutron scattering,[1] grazing incidence small-angle X-ray scattering (GISAXS),[2] ^{19}F-NMR,[3] etc. The structure of these PFSIs has been extensively investigated since 1980s. A series of SAXS papers dealing with swollen Nafion membranes were reported and various structure models were proposed, such as ionic-cluster, cluster-network, and core-shell models.[4–9] Among them, the cluster-network model proposed by Gierke et al.[5,6] has been accepted for years because it accounts not only for the SAXS results but also for the physical properties of ionomers, such as high proton conductivity. The cluster-network model is that perfluorosulfonate groups form an ionic cluster and the cluster is connected via small path to each other. Hsu and Gierke[7] also presented a theory of ion clustering of Nafion and connected it with the percolative aspects of ion transport. Later, Heitner–Wirguin surveyed studies on perfluorinated membranes from viewpoints of structure properties and applications.[10] The properties and structure of these membranes were mainly studied by SAXS, small-angle neutron scattering (SANS), NMR, ESR conductance, and IR spectroscopy. Special attention has been dedicated to the solutions of these membranes and recasting of new films and composite ones. He addressed also to various applications, such as fuel cells, alkali cells, electrolyzers and sensors. Recently, Schmidt–Rohr and Chen have quantitatively simulated small-angle scattering data of Nafion. They proposed the new model for explaining the diffusion mechanism of water and protons.[11]

Another key issue for application of PEFC is development of solid polymer electrode (SPE). Application of polymer films to electrodes was proposed by Ticiauelli et al.[12] They proposed

three methods used to attain high power densities in solid polymer electrolyte (SPE) fuel cell systems with low catalyst (Pt) loading; (i) use of a higher wt% Pt/C in the supported electrocatalysts, (ii) sputtering of a thin film of platinum, and (iii) a combination of the two methods. SPEs have several advantages: high power density, compactness, high performance by cost, quick and stable operation at low temperature (room temperature to 100°C), nonelectrolyte leakage, and so on, for applications such as transportation, portable power generators, and generators for on-site use (house and building), and are now being investigated worldwide. However, since the membrane does not penetrate into the electrodes as liquid electrolyte does, the electrodes have low catalyst (platinum) utilization or need high catalyst-loadings.

Uchida et al. solved this problem by a simple fabrication method for membrane/electrode assemblies in PEFC with high performance as well as an ideal structure of the reaction field in the catalyst layer.[13–17] They prepared PFSI colloids, in which both a good network of PFSI and uniformity of PFSIs on Pt particles were achieved with colloid formation of PFSI chains in specific organic solvents. The PFSI colloids were selectively adsorbed onto the carbon agglomerates with highly dispersed Pt particles on the surface, and a catalyst paste-formation followed. Today, electrodes of PEFCs are manufactured from "catalyst ink," consisting of carbon, platinum, water, and ionomers. Certainly, the performance of PEFCs depends greatly on their structure of SPEs. However, to our knowledge, a very few numbers of studies have been reported on structure investigation of catalyst inks.

SANS is a powerful tool for structural investigations of polymeric systems. In particular, aqueous systems are suitable for SANS, because use of deuterated solvents makes it easy to investigate the nanoscopic structure with high neutron contrast. By simply tuning the scattering contrast with D_2O/H_2O, fine structure of multicomponent or multiphase polymeric systems can be precisely determined. This method is called contrast-variation small-angle neutron scattering (CV-SANS). As reported elsewhere, CV-SANS allows one to decompose scattering intensity functions to partial scattering functions, which carry exclusive information on specific components in the system.[18,19] In this work, we carried out a detailed analysis of the structure of catalyst inks of fuel cells by CV-SANS and proposed a possible microstructure of catalyst ink in solutions.

EXPERIMENTAL

Samples

Various types of catalyst ink were prepared by mixing carbon powder, ionomer ionomer-A (PFSI type ionomer). Carbon (Vulcan(R) XC72, Cabot Corporation) was used as received. The primary particle size and the specific surface of the carbon were 300 Å and 117 $m^2\ s^{-1}$, respectively. Nafion® DE2020 (21% aq. Solution) (Du Pont) was also used as a reference samples. Ionomer-A is a PFSI type ionomer having a similar properties to that of Nafion® DE2020. The typical volume concentrations of the carbon, ϕ_C, ionomer, ϕ_B, and Pt, ϕ_{Pt}, were 0.01, 0.02, and 0.001, respectively. The average size of Pt was about 20 Å with distribution of 10–40 Å, similar to Figure 3(c) of the work by Yano et al.[20] The film thickness of Nafion® 117 membrane was 175 μm. The electrode thickness was 100 μm. The catalyst carbon processing was as follows; (1) dispersion of carbon black in water. If necessary, pH adjusting so as to attain uniform dispersion, (2) addition of chloroplatinic acid aqueous solution drop by drop to the dispersion, (3) reduction by adding either formic acid, formaldehyde, or alcohol, (4) rinsing and filtration, and (5) drying and heat treatment in the atmosphere of inert gas. In the case of catalyst in without Pt, the step (2) was skipped.

SANS

Small-angle neutron scattering experiments were carried out at SANS-U, Institute for Solid State Physics, the University of Tokyo. The wavelength of neutron was 7.0 Å. The sample-to-detector distances were chosen to be 2 and 12 m to cover a wide range of q, i.e., $3.0 \times 10^{-3}\ Å^{-1} \le q \le 3.0 \times 10^{-1}\ Å^{-1}$. Focusing optics was also employed to use a high-flux neutron (high-intensity mode) or to reach a very low q-range down to $3.0 \times 10^{-4}\ Å^{-1}$ (fine-focusing mode). As a result, a wide q-range, $3.0 \times 10^{-4}\ Å^{-1} \le q \le 3.0 \times 10^{-1}\ Å^{-1}$ could be covered in this work. In the case of the former, the incident flux of neutron beam was intensified by three times as that of a conventional pinhole collimation. The details of FSANS are described elsewhere.[21] Observed scattering intensity was corrected for cell scattering, transmission, and then scaled to the absolute scattering intensity with a secondary standard sample, low density polyethylene.[22]

RESULTS AND DISCUSSION

Overview Scattering and SANS for Polymer Electrodes

Figure 1 shows an overview of SANS patterns; (a) the scattering functions of polymer electrodes with and (b) without Pt, (c) Pt dispersion in water, (d) Nafion® membrane (Nafion 117), and (e) ionomer solution in D_2O ($\phi_P = 0.02$). Note that a small amount of ionomer was added for (c) in order to obtain homogenous dispersion of Pt. Note that the strong scattering for the polymer electrodes comes mainly from carbon agglomerates embedded in polymer, which are large and have enough contrast with respect to polymer ($3.95 \times 10^{10}\ cm^{-2}$) in neutron scattering. On the other hand, Nafion membrane itself was bulk (i.e., no solvent), which could be regarded as a single component system with a very small contrast for neutron scattering because ionic clusters are small and do not give significant contrast in bulk state. This is why the scattering intensity from Nafion membrane is very weak. As shown in the figures, the scattering functions from the polymer electrodes is a power-law function having a crossover around $q = 0.005\ Å^{-1}$ indicative of a fractal nature. It was found that no noticeable difference between polymer electrodes with and without Pt was observed. This is mainly due to the low concentration of Pt in the polymer electrodes. The asymptotes are about -1 and -4, respectively for the low ($q < 0.005\ Å^{-1}$) and high q regions. No significant effect by adding Pt was observed from the aspect of static structure. Scattering from Pt was not observed because of low concentration of Pt in the water dispersion. As shown in the figure, curves (a) and (b) could be fitted with Freltoft–

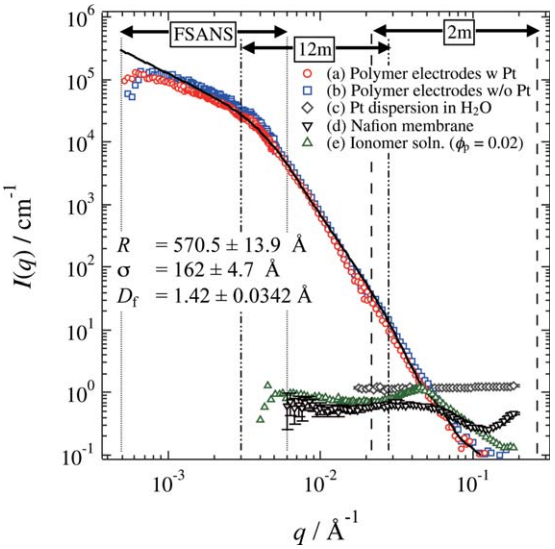

Figure 1. SANS functions, $I(q)$s, for (a) solid polymer electrode with Pt, (b) without Pt, (c) Pt dispersion in water, (d) ionomer (Nafion), and (e) ionomer solution in D_2O. [Color figure can be viewed in the online issue, which is available at wileyonlinelibrary.com.]

Kjems–Sinha (FKS) function.[23] FKS describes a scattering functions with a power-law correlations and finite-size effects in spherical particle agglomerates as given by,

$$S(q)=1+\frac{1}{(qR)^{D_m}}\frac{D_m\Gamma(D_m-1)}{\left[1+1/\left(q^2\xi^2\right)\right]^{(D_m-1)/2}}\sin\left[(D_m-1)\tan^{-1}(q\xi)\right] \quad (1)$$

Here, $\Gamma(x)$ is the Gamma function of x. D_m and ξ are the fractal dimension and the characteristic size of the mass fractal. The form factor for a spherical particle, $P_{\mathrm{sph}}(R, q)$ is given by

$$P_{\mathrm{sph}}(R,q)=\left[\Phi_{sph}(R,q)\right]^2 \quad (2)$$

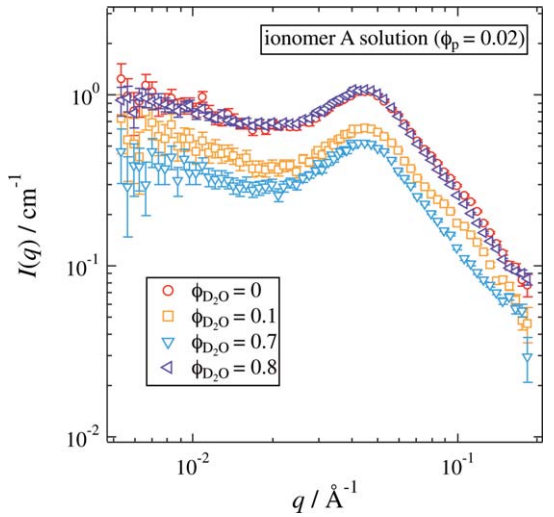

Figure 2. SANS functions of ionomer-A ($\phi_P = 0.02$) measured with various solvent compositions, ϕ_{D2O}. [Color figure can be viewed in the online issue, which is available at wileyonlinelibrary.com.]

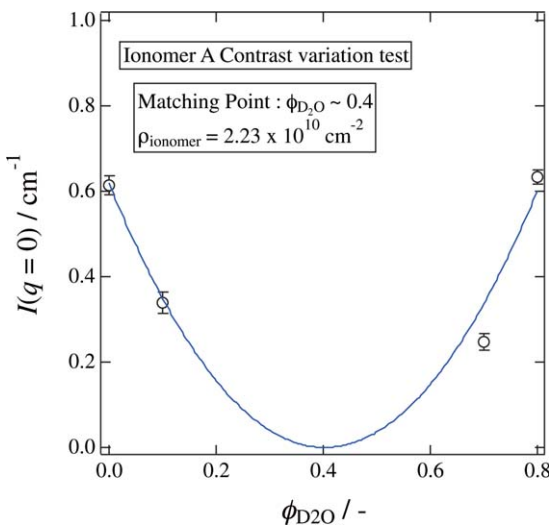

Figure 3. Plot of $I(q=0)$ for determination of the contrast-matching point for ionomer-A. [Color figure can be viewed in the online issue, which is available at wileyonlinelibrary.com.]

with

$$\Phi_{\mathrm{sph}}(R,q)=\frac{3[\sin(qR)-qR\cos(qR)]}{(qR)^3} \quad (3)$$

If the assembly of spheres has a size distribution, the above equation should be re-written to

$$P_{polydispersity}(q)=\int_0^\infty V^2G(R,x,\sigma)P_{\mathrm{sph}}(R,q)dx$$
$$G(R,x,\sigma)=\frac{1}{\sqrt{2\pi}\sigma}\exp\left(-\frac{(R-x)^2}{2\sigma^2}\right) \quad (4)$$

Here, we assumed a Gaussian distribution, and σ and V are the standard deviation and the volume of the particle with R, respectively. The solid line in the figure is a fitted function with FKS function. Because a change of slope (upper limit of agglomeration size) at low-q region was not observed, ξ was fixed ($= 1.00 \times 10^3$ Å) in this work. The fitted parameters are $R = 570.5$ Å, $\sigma = 162$ Å, $D_m = 1.42$. This means that carbon particles are sparsely agglomerated rather linearly ($D_m = 1.42$) in space at least up to a range of 1 μm (the lower limit of SANS observable range). The high ion conductivity of the polymer electrodes may be due to this fractal structure of carbon agglomerates.

CV-SANS

A series of SANS experiments were carried out for carbon dispersions and 2 vol % ionomer-A solutions with different compositions of D_2O/H_2O in order to evaluate the scattering length density (SLD) of each component. Figure 2 shows the case of ionomer-A ($\phi_P = 0.02$). Note that the SANS functions have a scattering maximum around $q = q_m \approx 0.05$ Å^{-1}. This peak is assigned to be a characteristic of polyelectrolytes as have been extensively discussed in the literature,[24–27] which is originated from the contrast between ion-rich (polymer-poor) and ion-poor (polymer-rich) domains/matrix. The observed scattering functions, $I(q)$, were fitted with a Gaussian function with an off-

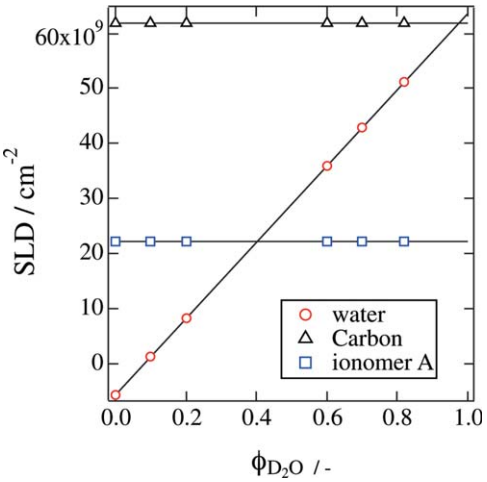

Figure 4. Variations of scattering length density (SLD) as a function of the solvent composition, ϕ_{D2O}. [Color figure can be viewed in the online issue, which is available at wileyonlinelibrary.com.]

set of $I(0)$ exclusively around to $q = q_m$ as shown with the solid line. Then, $I(0)$ was plotted as a function of ϕ_{D2O}, i.e., the fraction of D_2O as shown in Figure 3. The solid line is a fit with

$$I(q) \sim [\rho_P - \rho_W(\phi_D)]^2 \quad (5)$$

where ρ_P and ρ_W are the scattering length densities of the polymer (ionomer) and the solvent, respectively. From the minimum of the fitted function, the scattering length density (SLD) for ionomer-A was evaluated to be $\rho_P = 2.23 \times 10^{10}$ cm^{-2}. Similarly, SLDs of carbon and Nafion were obtained to be $\rho_C = 6.18 \times 10^{10}$ cm^{-2} and $\rho_P = 3.25 \times 10^{10}$ cm^{-2}, respectively. Figure 4 shows the SLDs for carbon (triangles), ionomer-A (squares), and the solvent (a mixture of D_2O and H_2O) (circles) as a function of the water compositions used for CV-SANS (open circles).

Figure 5 shows SANS functions of catalyst ink made of aqueous solutions of carbon ($\phi_C = 0.01$) and ionomer-A with various ϕ_{D2O}'s. For $\phi_{D2O} = 0$, $I(q)$ is a monotonic decreasing function of q, indicating carbon dominant scattering. $I(q)$ decreases significantly, and carbon only scattering was observed at $\phi_{D2O} = 0.4$. For $\phi_{D2O} > 0.4$, polymer scattering becomes dominant, characteristic of a scattering maximum around $q = 0.05$ Å^{-1}. Hence, it can be noted that $I(q)$ of catalyst ink is a sensitive function of ϕ_{D2O} not only for the magnitude but also for the shape of the function.

Singular value decomposition method was applied on the set of $I(q)$s shown in Figure 5. The singular value decomposition is described by the following equation,

$$\begin{pmatrix} I_1(q) \\ \cdots \\ \cdots \\ \cdots \\ I_1(q) \end{pmatrix} = \begin{pmatrix} C_{11} & .. & .. & C_{1m} \\ .. & .. & .. & .. \\ .. & .. & .. & .. \\ .. & .. & .. & .. \\ C_{n1} & .. & .. & C_{nm} \end{pmatrix} \begin{pmatrix} S_1(q) \\ \cdots \\ \cdots \\ S_m(q) \end{pmatrix} \quad (6)$$

$(n \times 1) \qquad (n \times m) \qquad (m \times 1)$

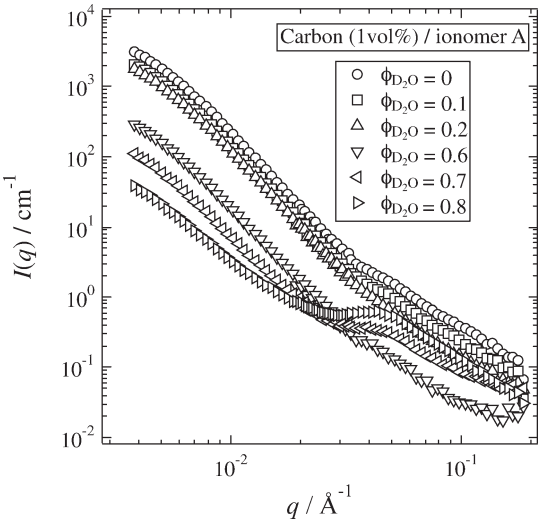

Figure 5. Series of SANS functions for catalyst ink with carbon and ionomer-A measured with different solvent compositions, ϕ_{D2O}. The concentrations of the catalyst ink were $\phi_C = 0.01$ and $\phi_P = 0.02$.

Here, the set of $I(q)$s, i.e., $[I_i(q)]$, are SANS intensity functions obtained with various scattering contrasts. $[C_{ij}]$ is the coefficient matrix of $n \times m$ ($n \geq m$), and $[S_j(q)]$ is the partial scattering function. Each element of the coefficient matrix corresponds to the scattering length density difference, i.e., $\Delta\rho_{ij}$. In principle, m–times SANS measurements are necessary for the determination of $[S_j(q)]$ ($j = 1, \ldots, m$). However, more numbers of measurements are necessary for precise determination of $[S_j(q)]$ because $I_i(q)$ carries statistical errors. In this work, we carried out 6 different SANS measurements for each sample to determine 3 $S_j(q)$'s, i.e., $S_{CC}(q)$, $S_{PP}(q)$, and $S_{CP}(q)$. The details of CV-SANS are described elsewhere.[18,19] Figure 6 shows a series of SANS functions; the observed (open circles) and reconstructed SANS functions (solid lines) for catalyst ink (carbon and ionomer-A). The reconstructed SANS functions well reproduce their original (observed) SANS functions, assuring the

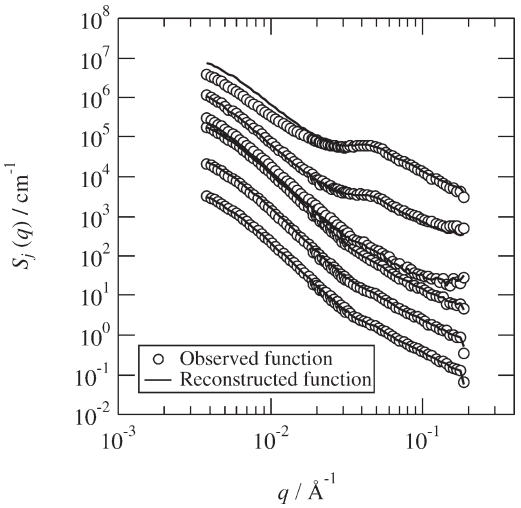

Figure 6. Observed (open circles) and reconstructed (solid lines) SANS functions for the catalyst ink with carbon and ionomer-A.

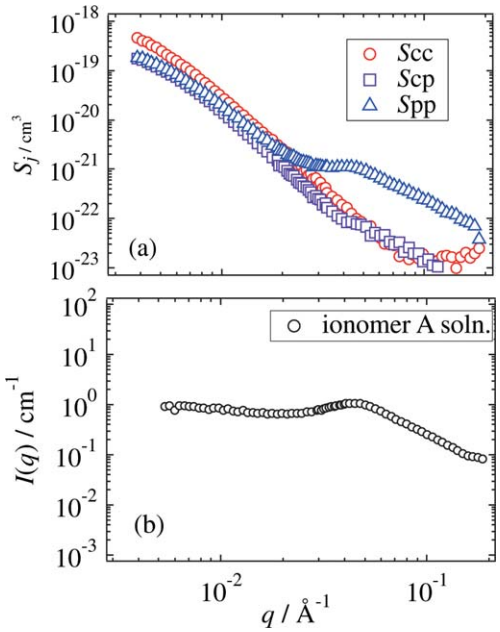

Figure 7. (a) Decomposed partial structure factors, $S_{CC}(q)$, $S_{PP}(q)$, and $S_{CP}(q)$. (b) SANS function of ionomer-A (2 vol %) solution. (b) The SANS function of the ionomer-A. [Color figure can be viewed in the online issue, which is available at wileyonlinelibrary.com.]

validity of the decomposition. Note that each SANS function was shifted vertically to avoid overlap.

Evaluation of Partial Structure Factors

Owing to precise determination of SLDs of the component and series of SANS measurements on catalyst inks, we succeeded in extraction of partial structure factors. Figure 7(a) shows three partial structure factors, $S_{CC}(q)$, $S_{PP}(q)$, and $S_{CP}(q)$. $S_{CC}(q)$ looks a monotonic decreasing function of q, whereas $S_{PP}(q)$ exhibits a clear scattering maximum around $q = 0.05$ Å^{-1} as pointed out above. Figure 7(b) shows SANS function of ionomer-A solution. It is noteworthy that it has a scattering maximum at the same q as that of $S_{PP}(q)$. In the following, we discuss these partial structure factors individually.

Figure 8 is a replot of $S_{CC}(q)$, i.e., the carbon scattering. The solid line is a fit with a scattering function for spheres. The partial structure factor for carbon agglomerates is given by

$$S_{CC}(q) = n_C V^2 P_{sph}(R, q) \tag{7}$$

Here, n_C and V are the number density of the spherical agglomerates and the volume of an agglomerate, respectively. As shown in Figure 8, the SANS intensity seems to be a convex upward function at low-q region. This indicates that a power-law behavior ascribed to fractal aggregation was not observed and large-scale aggregation of carbon agglomerates is suppressed. This result is explained such that the catalyst ink is a very dilute solution and the interaction between carbon agglomerates is weakened by absorption of ionomer-A. Here, all fitting parameters were fixed, ($n_C = \phi_C / V = 1.29 \times 10^{13}$ cm^{-3}, $R = 570.5$ Å and $\Delta R = \sigma = 162$ Å). Because the catalyst ink is a very dilute solution of carbon ionomer-A, it may be reasonable that $S_{CC}(q)$ directly exhibits the scattering of carbon agglomerates.

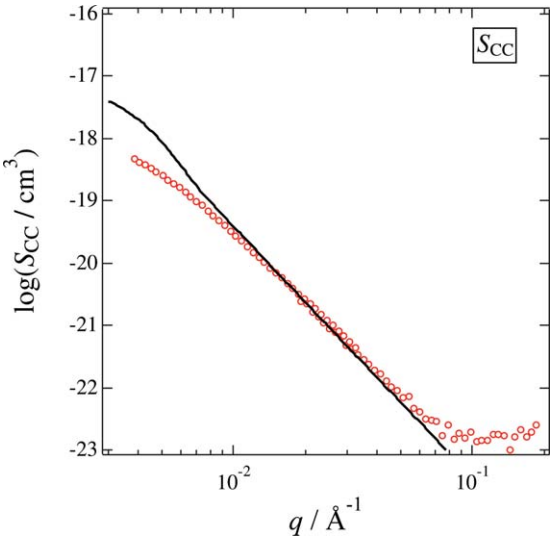

Figure 8. Result of curve fitting of $S_{CC}(q)$ with a scattering function for spherical particles. [Color figure can be viewed in the online issue, which is available at wileyonlinelibrary.com.]

Figure 9 shows $S_{CP}(q)$. The following equations were used for fitting.

$$\begin{aligned} S_{CP}(q) &= n_C \Phi_{sph} A_{coreshell}(q) \\ A_{coreshell}(q) &= \Delta\rho_{shell} V_{out} \Phi_{sph}(R_{out}, q) \\ &\quad -(\Delta\rho_{shell} - \Delta\rho_{core}) V_{core} \Phi_{sph}(R_{core}, q) \end{aligned} \tag{8}$$

Here, $A_{coreshell}$ is the scattering amplitude of a shell with outer and inner radii of R_{out} and R_{core}, respectively. In the process of curve fitting, the following parameters were fixed; the radius of core, $R_{core} = 570.5$ Å and the ionomer fraction in the medium $\phi_P^0 = 0.0184$ (in preparation). The evaluated set of parameters are $R_{shell} = 650$ Å, $\phi_{P,shell} = 0.35$, and $\phi_{P,matrix} = 0.018$.

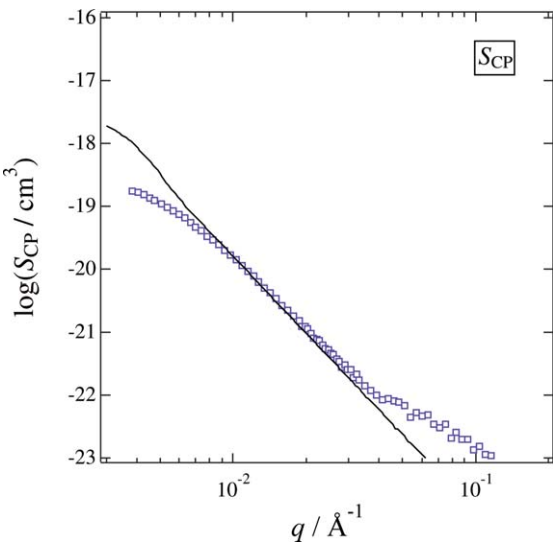

Figure 9. Result of curve fitting of $S_{CP}(q)$ with a scattering function for cross-term between spherical particles and core-shell particles. [Color figure can be viewed in the online issue, which is available at wileyonlinelibrary.com.]

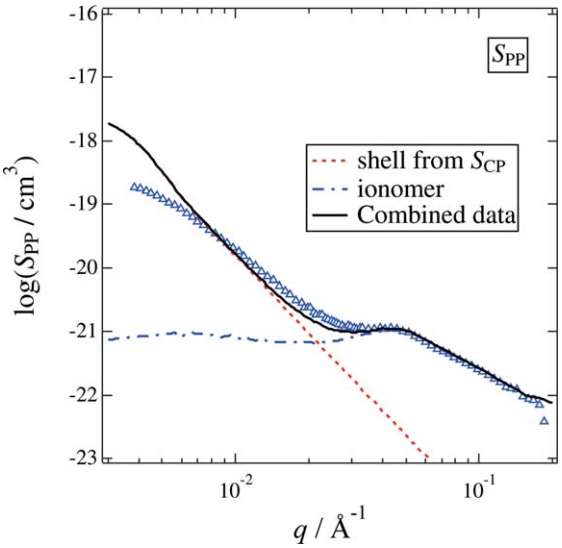

Figure 10. Result of curve fitting of $S_{PP}(q)$ (symbol; observed, solid line; calculated) with a scattering function for a combination of polyelectrolyte solutions (chain line) and core-shell particles (dotted line). The SANS function of the ionomer-A can be superimposed to $S_{PP}(q)$ for $q \geq 0.03$ Å^{-1}, indicating that the ionic structure in the catalyst ink is the same as in the corresponding ionomer-A solution. [Color figure can be viewed in the online issue, which is available at wileyonlinelibrary.com.]

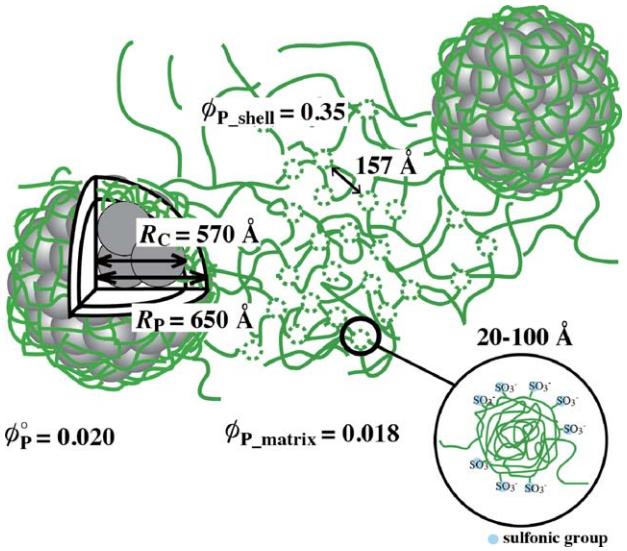

Figure 11. Schematic illustration of the structure of catalyst ink (dilute solution). Significant amount of ionomer chains are adsorbed on the surface of carbon agglomerates and there are concentration fluctuations of the spacing being about 150 Å due to the nature of polyelectrolyte in aqueous solution. [Color figure can be viewed in the online issue, which is available at wileyonlinelibrary.com.]

Figure 10 shows $S_{PP}(q)$, which is characterized by the scattering maximum at $q = 0.05$ Å^{-1}. As pointed out before, this type of scattering maximum has been observed in polyelectrolyte solutions. The chain line indicates the SANS function of ionomer-A solution. It well reproduces a part of $S_{PP}(q)$ for $q \geq 0.03$ Å^{-1}, whereas a steep upturn is observed exclusively in $S_{PP}(q)$. Hence, we tried to reconstruct $S_{PP}(q)$ with a sum of $S_{ionomer}(q)$ (chain line) and shell scattering calculated from fitting results of $S_{CP}(q)$ (dashed line). The reconstructed SANS function is shown with the solid line, which well reproduces $S_{PP}(q)$. This means that the $S_{PP}(q)$ consists of ionomer scattering (matrix) and a layer scattering adsorbed strongly on carbon agglomerates. This is why the upturn appears in $S_{PP}(q)$ in a low-q region and is well represented by considering a contribution of cross-term, $S_{CP}(q)$.

Regarding the ionomer scattering, Borue–Erkhimovich proposed a scattering function for weakly charged polyelectrolyte solutions on the basis of random phase approximation.[28] The structure factor is given by

$$S(x) = S^0(x)\left[1 - \frac{S^0(x)}{S^0(x) + (x^2 + s)}\right] \tag{9}$$

where x and s are the reduced scattering vector and the reduced salt concentration, respectively, as defined by

$$x \equiv r_0 q, \qquad s \equiv \kappa^2 r_0^2, \qquad r_0 = a\left(\frac{48\pi l_B \phi f^2}{a}\right)^{-1/4} \tag{10}$$

The parameter r_0 is the characteristic screening length of Coulombic interaction by ideal Gaussian chains. κ is the inverse of Debye screening length (l_D), l_B is the Bjerrum length ($\approx$ 7Å in water) and a is the monomer length, and ϕ is the fraction of the polyelectrolyte in solution. $S^0(x)$ is the structure factor for uncharged polymer solutions, written by

$$S^0(x) = \frac{1}{x^2 + t} \tag{11}$$

The variable t is the reduced temperature related to the Flory's interaction parameter χ as defined by,

$$t = 12\left(\frac{r_0}{a}\right)^2\left[(1 - 2\chi)\phi + \frac{3B_3}{a^3}\phi^2\right] \tag{12}$$

Here, B_3 is the 3rd virial coefficient. Shibayama et al. applied this theory to characterize weakly charged polymer gels.[29,30] By employing this theory, we obtained the structure parameters, $a = 25.603$, $r_0 = 22.189$ Å, $l_D = 77.519$ Å, $\chi = 0.54307$. Muthukumar proposed a more elaborated theory for polyelectrolyte solutions.[31] The discussion on the scattering maximum, however, is beyond the scope of this work.

Possible Model of Catalyst Ink

On the basis of the experimental results and related discussions, we propose a structure model for the catalyst ink in a dilute solution, which is shown in Figure 11. The major component is the carbon agglomerates of core radius ca 570 Å and outer shell radius of ca 670 Å. In this shell region, ionomer chains are heavily adsorbed and its concentration is $\phi_{P,shell} \approx 0.35$, which is much higher than that in the matrix, $\phi_{P,matrix} \approx 0.018$ and that at preparation, $\phi_P{}^0 \approx 0.020$. The characteristic distance of polyelectrolyte solutions of ca. 150 Å is seen due to concentration fluctuations in ion-rich and -poor domains. During solvent evaporation process, the adsorbed layers are shrunken and a phase inversion occurs from the polymer-poor matrix and -rich domains to polymer-poor domains in polymer-rich matrix. Furthermore, polymer-poor domains (i.e., ionic cluster) interconnected and form a percolated path for protons. As a result, ionic-cluster networks

are formed. This model for catalyst ink can be satisfactorily extrapolated to those models proposed in the literature.[5]

CONCLUSION

Contrast-variation small-angle neutron scattering (CV-SANS) experiments were carried out in order to elucidate the structure of catalyst ink of fuel cells. First, the contrast matching points were carefully determined for Nafion, ionomer-A, and carbon. The CV-SANS revealed the following facts: (1) The microscopic structure of the catalyst ink consists of carbon agglomerates surrounded by ionomers. (2) The SANS function of ionomer solutions have an ionic cluster peak around $q \approx 0.05\text{Å}^{-1}$, which maintain its structure even in the ink mixed with carbon/Pt. (3) The cross term, i.e., $S_{CP}(q)$, indicates a percolated structure of carbon clusters mediated by ionomers. During solvent evaporation process on a separator membrane, the adsorbed layers are shrunken and a phase inversion occurs. This leads to formation of interconnected ionic-cluster networks with percolated paths for proton conduction. Hence, the presence of this ionic-cluster path seems to play a key role in the performance of the solid polymer electrodes in polymer electrolyte fuel cells.

ACKNOWLEDGMENTS

This work was carried out under the Joint-use Research Program for Neutron Scattering, Institute for Solid State Physics (ISSP), the University of Tokyo, at the Research Reactor JRR-3, JAEA (Proposal No. 9404, 9598, and 10404).

REFERENCES

1. Gebel, G.; Diat, O. *Fuel Cells* **2005**, *5*, 261.
2. Bass, M.; Berman, A.; Singh, A.; Konovalov, O.; Freger, V. *Macromolecules* **2011**, *44*, 2893.
3. Ma, S.; Chen, Q.; Jøgensen, F. H.; Stein, P. C.; Skou, E. M. *Solid State Ionics* **2007**, *178*, 1568.
4. Gierke, T. D.; Munn, G. E.; Wilson, F. C. *J. Polym. Sci. Polym. Phys. Ed.* **1981**, *19*, 1687.
5. Gierke, T. D.; Hsu, W. Y. Perflnorinated Ionomer Membranes; ACS Symposium Series. Washigton DC, 1982.
6. Hsu, W. Y.; Gierke, T. D. *J. Membr. Sci.* **1983**, *13*, 302.
7. Hsu, W. Y.; Gierke, T. D. *J. Membr. Sci.* **1983**, *13*, 307.
8. Hashimoto, H.; Fujimura, M.; Hashimoto, T.; Kawai, H. *Macromolecules* **1981**, *14*, 844.
9. Fujimura, M.; Hashimoto, T.; Kawai, H. *Macromolecules* **1982**, *15*, 136.
10. Heitner-Wirguin, C. *J. Membr. Sci.* **1996**, *120*, 1.
11. Schmidt-Rohr, K.; Chen, Q. *Nat. Mater.* **2008**, *7*, 75.
12. Ticiauelli, E. A.; Derouin, C. R.; Srinivasau, S. *J. Electroanal. Chem.* **1988**, *251*, 275.
13. Uchida, M.; Aoyama, Y.; Eda, N.; Ohta, A. J. *Electrochem. Soc.* **1995**, *142*, 463.
14. Uchida, M.; Aoyama, Y.; Eda, N.; Ohta, A. J. *Electrochem. Soc.* **1995**, *142*, 4143.
15. Uchida, M.; Fukuoka, Y.; Sugawara, Y.; Eda, N.; Ohta, A. J. *Electrochem. Soc.* **1996**, *143*, 2245.
16. Uchida, M.; Fukuoka, Y.; Yasushi Sugawara, Y.; Ohara, H.; Ohta, A. *J. Electrochem. Soc.* **1998**, *145*, 3708.
17. Uchida, M.; Kurosaka, M.; Osada, Y. *Macromolecules* **1995**, *28*, 4583.
18. Endo, H.; Schwahn, D.; Cölfen, J. *J. Chem. Phys.* **2004**, *120*, 9410.
19. Miyazaki, S.; Endo, H.; Karino, T.; Haraguchi, K.; Shibayama, M. *Macromolecules* **2007**, *40*, 4287.
20. Yano, H.; Akiyama, T.; Bele, P.; Uchida, H.; Watanabe, M. *Phys. Chem. Chem. Phys.* **2010**, *12*, 3806.
21. Iwase, H.; Endo, H.; Katagiri, M.; Shibayama, M. *J. Appl. Cryst.* **2011**, *44*, 558.
22. Shibayama, M.; Matsunaga, T.; Nagao, M. *J. Appl. Cryst.* **2009**, *42*, 621.
23. Freltoft, T.; Kjems, J. K.; Sinha, S. K. *Phys. Rev. B.* **1986**, *33*, 269.
24. Nierlich, M.; Williams, C. E.; Boué, F.; Cotton, J. P.; Daoud, M.; Farnoux, B.; Jannink, G.; Picot, C.; Moan, M.; Wolff, C.; Rinaudo, M.; de Gennes, P. G. *J. Phys. (Paris)* **1979**, *40*, 701.
25. Ise, N.; Okubo, T.; Yamamoto, K.; Kawai, H.; Hashimoto, T.; Fujimura, M.; Hiragi, Y. *J. Am. Chem. Soc.* **1980**, *102*, 7901.
26. Schosseler, F.; Ilmain, F.; Candau, S. *J. Macromolecules* **1991**, *24*, 225.
27. Schosseler, F.; Moussaid, A.; Munch, J. P.; Candau, S. J. *J. Phys. II France 1* 1991, 1197.
28. Borue, V.; Erukhimovich, I. *Macromolecules* **1988**, *21*, 3240.
29. Shibayama, M.; Tanaka, T.; Han, C. C. *J. Chem. Phys.* **1992**, *97*, 6842.
30. Shibayama, M. In Soft Matter Characterization; Pecora, P., Borsali, R., Eds.; Springer-Verlag, **2008**; Chapter 14. pp. 783–832, Meppel, The Netherlands.
31. Muthukumar, M. *Macromolecules* **2002**, *35*, 9142.